reflections, 496 parameters, $R = 0.0633$. **4**: Triclinic, $P\bar{1}$, $a = 10.689(2)$, $b = 11.170(2)$, $c = 15.330(6)$ Å, $\alpha = 84.2(3)$, $\beta = 89.39(3)$, $\gamma = 73.24(3)^\circ$, $V = 1743.3(6)$ Å^3, $Z = 2$, 3849 "observed" reflections, 356 parameters, $R = 0.0373$. The hydride hydrogen atom H(a) was localized by differential Fourier synthesis and refined with a free isotropic B value. **5**: Monoclinic, $C2/c$, $a = 25.090(5)$, $b = 10.798(2)$, $c = 30.262(6)$ Å, $\beta = 106.99(3)^\circ$, $V = 7841(3)$ Å^3, $Z = 8$, 4103 "observed" reflections, 370 parameters, $R = 0.0598$. Further details of the crystal structure investigations may be obtained from the Fachinformationszentrum Karlsruhe, D-76344 Eggenstein-Leopoldshafen, Germany (fax: (+49)7247-808-666; e-mail: crysdata§fiz-karlsruhe.de) on quoting the depository numbers CSD-133780 (**3**), -133781 (**4**), and 133782 (**5**).

[16] C. Brelière, F. Carré, R. J. P. Corriu, G. Royo, *Organometallics* **1988**, *7*, 1006 – 1008.

[17] M. J. Barrow, E. A. V. Ebsworth, M. M. Harding, D. W. H. Rankin, *J. Chem. Soc. Dalton Trans.* **1980**, 603 – 606.

[18] M. Lazraq, J. Escudié, C. Couret, J. Satgé, M. Dräger, R. Dammel, *Angew. Chem.* **1988**, *100*, 885 – 887; *Angew. Chem. Int. Ed. Engl.* **1988**, *27*, 828 – 830.

[19] T. S. Cameron, K. M. Mannan, S. R. Strobert, *Cryst. Struct. Commun.* **1975**, *4*, 601.

[20] W. P. Freeman, T. D. Tilley, F. P. Arnold, A. L. Rheingold, P. K. Gantzel, *Angew. Chem.* **1995**, *107*, 2029 – 2031; *Angew. Chem. Int. Ed. Engl.* **1995**, *34*, 1887 – 1890.

[21] P. B. Hitchcock, N. H. Buttrus, A. C. Sullivan, *J. Organomet. Chem.* **1986**, *303*, 321 – 327.

[22] K. J. Weese, R. A. Bartlett, B. D. Murray, M. M. Olmstead, P. P. Power, *Inorg. Chem.* **1987**, *26*, 2409 – 2413.

[23] J. Hvoslef, H. Hope, B. D. Murray, P. P. Power, *J. Chem. Soc. Chem. Commun.* **1983**, 1438 – 1439.

[24] B. Bogdanović, C. Krüger, B. Wermeckes, *Angew. Chem.* **1980**, *92*, 844 – 845; *Angew. Chem. Int. Ed. Engl.* **1980**, *19*, 817 – 818.

[25] M. Motevalli, D. Shah, A. C. Sullivan, *J. Chem. Soc. Dalton Trans.* **1993**, 2849 – 2855.

[26] M. Veith, M. Nötzel, L. Stahl, V. Huch, *Z. Anorg. Allg. Chem.* **1994**, *620*, 1264 – 1270.

[27] C. Glidewell, M. B. Hursthouse, D. Lloyd, K. W. Lumbard, R. L. Short, *J. Chem. Res.* (*S*) **1986**, 400 – 401.

[28] A. Schäfer, W. Saak, M. Weidenbruch, H. Marsmann, G. Henkel, *Chem. Ber.* **1997**, *130*, 1733 – 1737.

[29] M. Veith, S. Becker, V. Huch, *Angew. Chem.* **1989**, *101*, 1287 – 1288; *Angew. Chem. Int. Ed. Engl.* **1989**, *28*, 1237 – 1238.

Crystal Design of Barium Sulfate using Double-Hydrophilic Block Copolymers

Limin Qi, Helmut Cölfen and Markus Antonietti*

The controlled growth of crystals with respect to size, shape, and crystal structure, the so-called "crystal design", is a preindustrial manufacturing procedure known since the Middle Ages, but has returned as a key aspect of modern materials science. The reasons for this are obvious, since the use of powders as abrasives, fillers, or ceramic precursors relies on the homogeneity of the powders to certain particle sizes and shapes. Further, the patterns of bioceramic matter such as bone, teeth, or seashells, with their properties superior to current man-made ceramics, show that control of the growth of single nanocrystals as well as their simultaneous alignment in some ordered superstructure is a motive to generate water-borne, environmentally friendly materials.[1] In this Communication, biological principles to control crystal growth are mimicked with easily synthesized polymers where the growth of $BaSO_4$ is affected to effect a wide variety of well-defined morphologies.

The morphology of single nanocrystals or colloidal microparticles is classically controlled by application of low molecular mass additives or salts, hydrothermal hydrolysis of amorphous solids, or special crystallization conditions.[2] In recent years, biological molecules were isolated from living systems, for example from seashells, and the crystal growth control was repeated in in-vitro experiments.[3] Recently, a new class of crystal modifiers, the double-hydrophilic block copolymers, was developed[4a] and found to be very active in the control of the crystal morphologies of calcium carbonate[4a, 5] and hydroxyapatite.[6] Those polymers are designed as "molecular tools", where one block interacts strongly with the mineral surface whereas the other block just keeps the "construction site" in solution. In this work, we report on the control and generation of unconventional crystal superstructures of barite, $BaSO_4$, using such block copolymers.

We varied the functional polymer block over a broad range, building polymer-bound arrays of carboxylate groups, aspartic acids, sulfonates, and phosphonates. Poly(ethyleneglycol)-*block*-poly(ethyleneimine)-poly(acetic acid) (PEG-*b*-PEIPA, PEG = 5000 g mol^{-1}, PEIPA = 1800 g mol^{-1}) was obtained as described in ref. [4a]. Poly(ethyleneglycol)-*block*-poly(ethyleneimine)-poly(sulfonic acid) (PEG-*b*-PEIPSA, PEG = 5000 g mol^{-1}, PEIPSA = 2360 g mol^{-1}) was prepared similarly by quantitative reaction with 1,3-propanesultone[4b]. A commercial poly(ethyleneglycol)-*block*-poly(methacrylic acid) (PEG-*b*-PMAA, PEG = 3000 g mol^{-1}, PMAA = 700 g mol^{-1}; Goldschmidt AG) was used as received. PEG-*b*-PMAA-Asp, with amino acid side chains, was prepared by amidation of PEG-*b*-PMAA with aspartic acid (27%),[4b] while PEG-*b*-PMAAP was prepared by partially monophosphonating (21%) the COOH groups of PEG-*b*-PMAA[5]. All polymers were purified by exhaustive dialysis. Crystal modification data is presented for these five double-hydrophilic block copolymers together with poly(methacrylic acid) (PMAA, as sodium salt; Aldrich, PMMA = 6500 g mol^{-1}).

The "synthesis" of the $BaSO_4$ particles involves simultaneous addition of 0.5 M $Ba(OAc)_2$ (Aldrich), 0.5 M $(NH_4)_2SO_4$ (Aldrich), and a 1 g L^{-1} aqueous solution of the different polymers (at pH 5 unless otherwise specified) in a double-jet reactor[4a] maintained at 25 °C. The continuous reactant supply of 0.5 mL h^{-1}, leading to a $BaSO_4$ formation rate of 1.39×10^{-5} mol L^{-1} min^{-1}, was stopped when the solution became turbid or crystal formation could be observed. The precipitates were left to stand in their mother solutions for at least 24 h to ensure equilibration.

The resulting $BaSO_4$ precipitates were characterized by scanning electron microscopy (SEM), and by transmission

[*] Prof. Dr. M. Antonietti, Dr. L. Qi, Dr. H. Cölfen
Max-Planck-Institut für Kolloid- und Grenzflächenforschung
Am Mühlenberg, Golm
14424 Potsdam (Germany)
Fax: (+49) 331-567-9502
E-mail: pape@mpikg-golm.mpg.de

  0570-0833/00/3903-0604 $ 17.50+.50/0

electron microscopy (TEM) (SEM: DSM 940 A, TEM: EM 912 Omega, Carl Zeiss, Jena). Dry powder samples were used for the measurements of X-ray powder diffraction (XRD) using PDS 120 unit and Cu Kα radiation (Nonius GmbH, Solingen), and thermogravimetry (TG) on a Netzsch TG 209 unit (Selb, Germany). The obtained XRD patterns were indexed with reference to the unit cell of the barite structure ($a = 8.87$, $b = 5.45$, $c = 7.15$ Å, space group *Pnma*).[7] The crystallite sizes of the $BaSO_4$ particles were estimated from the half-height width of the barite-(211) peak according to the Scherrer equation.

The control precipitation experiment, at pH 7 without an additive, yielded rectangular $BaSO_4$ crystals of about 0.6 μm length with a mean aspect ratio of 1.2 (Figure 1 a). Similar

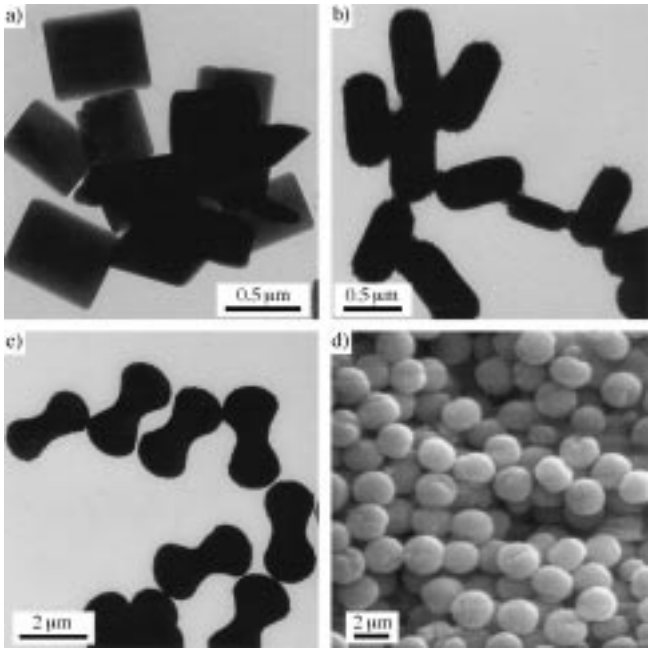

Figure 1. $BaSO_4$ particles formed in the presence of a) no additives, b) PMAA, c) PEG-*b*-PEIPA, and d) PEG-*b*-PMAA-Asp, observed by TEM (a – c) and SEM (d). $BaSO_4$ particles show various morphologies such as rectangular tablets (a), rods (b), peanuts (c), and peaches (d).

tablets were obtained at pH 5 and pH 9, although severe aggregation was observed at pH 9. These tablets are similar to those of $BaSO_4$ crystallized from a supersaturated solution under static growth conditions, each of which was a single crystal elongated along the [001] crystallographic axis.[8] However, the $BaSO_4$ tablets obtained here are smaller, presumably because double-jet precipitation results in fast nucleation and many small crystals.

The obtained products precipitated in presence of PMAA at pH 5 are elongated particles with an average length of 0.8 μm and an aspect ratio of about 2.1 (Figure 1 b). The rough surface of the rods indicates that they consist of primary crystallites, corresponding to XRD evidence of a mean crystal size of 22 nm. The overall shape implies that the superstructure is composed of rod-like crystallites aligned along the rod axes. This result on the simple polymer suggests a significant interaction between the polymeric pattern of carboxylic acid groups and the crystallizing $BaSO_4$, resulting in the considerable influence on both the primary crystallization as well as on the superstructure.

If a similar functional block is connected to an inert, soluble PEG block to form the additive PEG-*b*-PMAA, a new overall morphology is formed. At pH 9, a peanutlike morphology (similar to Figure 1 c but only 0.8 μm long) composed of 14 nm primary crystallites (XRD) is found, whereas at pH 5, peachlike, 2 μm sized particles of 18 nm primary crystallites (XRD) were obtained, very similar to those shown in Figure 1 d. This result illustrates that incorporation of a solubilizing block into the template structure is also important for the crystal morphology. Obviously, stabilization of the primary crystallites and their subsequent aggregation into a macrostructure are facilitated by the block copolymer structure.

As shown in Figure 1 c, well-defined peanutlike particles around 3.0 μm in size are also obtained with PEG-*b*-PEIPA as a modifier at pH 5. Using PEG-*b*-PMAA-Asp at the same pH results again in uniform peachlike particles of an average 2.3 μm size (Figure 1 d). In this case, the equatorial depression of the particular superstructure becomes visible. The corresponding XRD results showed that both the peanuts and the peaches consist of barite primary crystallites (27 nm for PEG-*b*-PEIPA and 19 nm for PEG-*b*-PMAA-Asp).

It is interesting to note that similar peanutlike particles of hematite (α-Fe_2O_3) have been produced by a gel-sol method in the presence of sulfate ions.[9] It has been reported that sulfate restrained the growth in all directions normal to the *c* axis of hematite resulting in crystalline rods, whereas the peanut superstructure is the product of the aggregation of these rods directed by specific forces.[9, 10] In the present case, it is assumed that the COOH groups of both PEG-*b*-PMAA and PEG-*b*-PEIPA play a similar role restricting crystallization of $BaSO_4$ in all directions but one, where directional aggregation of the rodlike primary crystallites leads to peanutlike particles. Our preliminary TEM studies on thinly cut samples confirmed the presence of nanometer-sized rodlike crystallites in the peanutlike $BaSO_4$ particles, supporting the proposed building mechanism.

It is further speculated that Figures 1 b – d represent different stages of the directed aggregation of $BaSO_4$ nanorods in a process which has been described in detail for the formation of fluorapatite superstructures in a gelatin matrix.[11, 12] In a like manner, the peanut shape is explained by electrical field lines of a primary rodlike crystallite (see Figure 1 b) which directs the aggregation of further crystallites. This was again confirmed by TEM of thin cuts of the peanutlike macrostructures which showed the primary crystallites are aligned along field lines (data not shown). Further growth at the caps of the peanut structure yield a sphere with an equatorial depression, such as the peaches, in analogy to similarily composed fluorapatite particles.[11]

Thermogravimetry has revealed that the final superstructures contain a small, but relevant, amount of polymer (5 – 12 wt-%) embedded between the primary $BaSO_4$ crystallites. The fact that the superstructures do not fall apart, even if ultrasound or good solvents for PEG are applied, suggests that the polymer acts as a binder for the different primary

  0570-0833/00/3903-0605 $ 17.50+.50/0

crystallites. This binding appears to be stronger than in the case of calcium minerals, as similar $CaCO_3$ particles can fall apart into the primary crystallites upon ultrasonication.

Phosphonation of the carboxylic acid groups of PEG-*b*-PMAA leads to a remarkable variation in the morphology of the $BaSO_4$ particles, namely, large bundles of nanofibers of $BaSO_4$ are produced. Many bundles of fibers show lengths of some tens of micrometers, most of which exhibit clear starting points. Appearances that include snails, bananas, and cones, can be observed. Figure 2a depicts a SEM image showing a

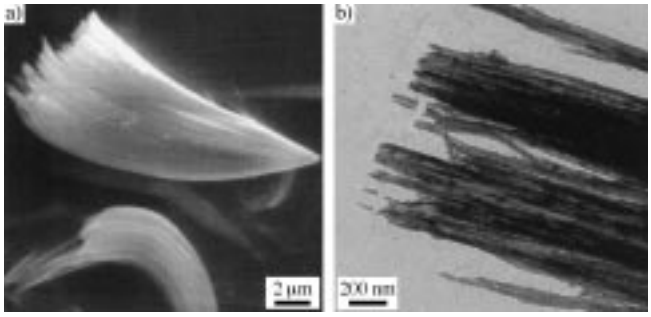

Figure 2. Micrographs of $BaSO_4$ particles formed in the presence of PEG-*b*-PMAAP observed using a) SEM and b) TEM. The high-magnification images show the structure as bundles of nanofibers.

conelike bundle of $BaSO_4$ nanofibers. The common starting points of the nanofibers suggest that they could be formed by heterogeneous nucleation from single centers (e. g., on the connection point between the two reactant jets or at the glass wall of the reaction vessel) followed by crystal growth along a single crystal direction. This can again be achieved by selective blocking of the crystal growth of all faces parallel to one axis by polymer adsorption. The corresponding TEM image of a thin slice shown in Figure 2b confirms the presence of bundles of nanofibers and shows that the fibers forming bundles are rather uniform in diameter (20 – 30 nm). The corresponding XRD pattern of these nanofibers exhibits relatively sharp barite scattering peaks, which gives for the main (211) peak an average crystallite size of about 60 nm, which is close to the resolution of the diffractometer. This result strongly indicates the single crystal structure of each fiber.

A better insight how the polymer interacts with the primary crystallites and how the morphology is controlled is gained by electron diffraction on very thin samples. We were not able to microtome the bigger particles, but microtoming of the nanofibers was possible. Figure 3a presents a TEM image of a thin section of a $BaSO_4$ nanofiber bundle formed in the presence of PEG-*b*-PMAAP. The section has been cut nearly along the fiber axis, resulting in an area of long continuous nanofibers that are aligned nearly parallel and exhibit rather uniform diameters (20 – 30 nm). The corresponding electron diffraction pattern (Figure 3b) consists of elongated but individual diffraction spots, most of which can be indexed as the reflections corresponding to the [001] zone of barite. It can be seen that the (210) reflection is located along the direction normal to the fiber axis, suggesting that the fiber axis is along the crystallographic [1$\bar{2}$0] axis. It is noteworthy that a few

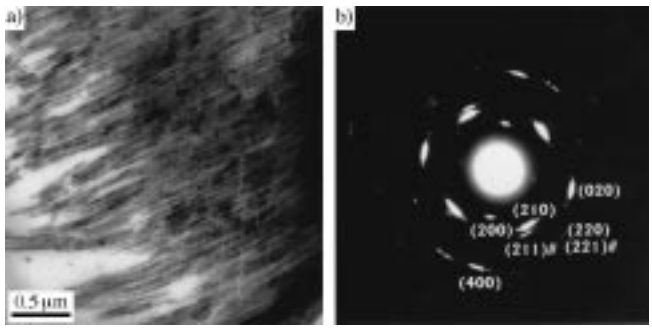

Figure 3. a) TEM micrograph and b) electron diffraction pattern of a thin section of a bundle of $BaSO_4$ nanofibers, formed in the presence of PEG-*b*-PMAAP, cut nearly along the fiber axis. The diffraction pattern corresponds to the upper-right region of (a), containing continuous, approximately parallel nanofibers. All indexed reflections correspond to the [001] zone of barite except the reflections labeled "#". The observation that the (210) reflection is located normal to the fiber axis suggests that the fibers are elongated along the [1$\bar{2}$0] axis.

reflections corresponding to other zones are also present in the whole diffraction pattern due to a degree of rotation of some fibers around their own axes. Specifically, reflections (211) and (221) accompany reflections (210) and (220), respectively. That the (211) reflection is also located normal to the fiber axis confirms that the fibers are elongated along the [1$\bar{2}$0] axis. The absence of symmetry in the diffraction pattern with respect to the [1$\bar{2}$0] axis indicates that the individual fibers cannot randomly rotate around their axes. This implies that these nanofibers assembled into a single bundle are vectorially aligned, and either geometric packing or force fields result in a high degree of correlation between the fibers with respect to the crystallographic direction. Further, that the nanofibers are elongated along the [1$\bar{2}$0] axis indicates that the PEG-*b*-PMAAP copolymer preferentially adsorbs on the faces parallel to the [1$\bar{2}$0] axis, such as (001), (210), and (211).

This remarkable interaction between PEG-*b*-PMAAP and the growing $BaSO_4$ particles is attributed to the specific pattern of the phosphonate groups along the polymer backbone. It is well known that (poly)phosphonate-type additives are effective inhibitors for the crystallization of barite.[13, 14] Indeed the presence of PEG-*b*-PMAAP delayed the precipitation of $BaSO_4$ significantly. For example, macroscopic crystal formation with PEG-*b*-PMAAP was not be observed until 180 min, whereas the same solution with PMAA and the carboxylic acid-containing block copolymers became turbid in less than 50 min. It was also observed that only a small amount of large fibers was formed when the injection of reactants was stopped at 180 min, and the majority of fibers form gradually under static conditions. This finding indicates that a metastable, inhibited $BaSO_4$ species is kept in solution at rather high concentrations (strong inhibition effect with PEG-*b*-PMAAP), which subsequently slowly recrystallizes to the observed large bundles of $BaSO_4$ fibers.

It is noteworthy that similar nanofibers of $BaSO_4$ have also been synthesized in reverse microemulsions, consisting of a continuous oil phase and water droplets stabilized by the surfactant AOT (sodium 5,14-diethyl-8,11-dioxo 7,12-dioxaoctadecane-2-sulfonate).[15] In this case, the reaction solutions

  0570-0833/00/3903-0606 $ 17.50+.50/0

were also initially transparent and became cloudy over a relatively long period, indicating a similar formation mechanism of the nanofibers.

A striking flowerlike morphology was obtained by the precipitation of $BaSO_4$ in presence of the sulfonated derivative PEO-*b*-PEIPSA, revealing the remarkable influence of the nature of the functional groups of the double-hydrophilic copolymers. As shown in Figure 4a, the flowerlike particles

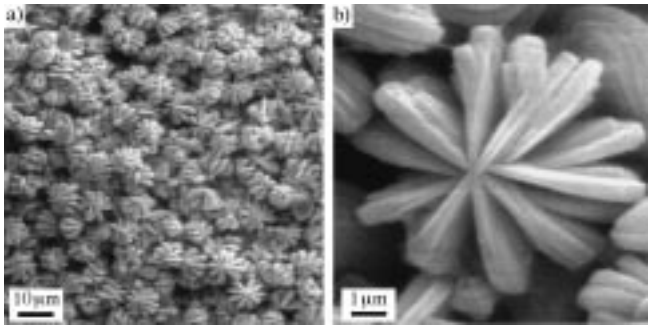

Figure 4. SEM micrographs of $BaSO_4$ particles, formed in the presence of PEG-*b*-PEIPSA, shows a) flowers with ten petals and b) enlarged to show details of a single flower.

are regular and rather uniform in size and shape, most of which are about 10 μm in size and have ten petals. Figure 4b presents a high-magnification image of a single particle.

It can be seen that the flower shows faceted surfaces, indicating that it is composed of large crystals. This is consistent with the XRD pattern which exhibited sharp barite diffraction peaks. The mechanism of the flower formation can again only be explained by selective adsorption of the polymer. In a first step, it is assumed that a rodlike primary crystal is formed (the axis of the flower). In a second step, these primary crystals nucleate secondary crystals which grow along ten of the directions perpendicular to the rod axis which are only weakly blocked by PEG-*b*-PEIPSA (role of the strength of adsorption). Finally, the sides of the petals are overgrown with secondary crystalline layers.

The role of the polymer on the resulting crystal morphology must be stressed to explain the variations observed for barite crystals. The exposed faces of barite crystals do show different polarity patterns and averaged interface energies, and adsorb the variously modified polymers with different efficiencies. A polymer-modified crystal grows into the direction where the crystallization hindrance is weakest, and fibers are formed when all but two sites are blocked. Peanut- and peachlike morphologies result from the parallel alignment of several crystalline rods to form rodlike particles in the micron range, where aggregation seems inhibited or even vectorially controlled by local electric fields, and the overall morphology is obtained depending on the strength of the dipole contribution. In contrast, stopping the primary growth and having secondary growth exclusively at the sides of the primary rod results in the flowerlike morphology.

In summary, it has been demonstrated that double-hydrophilic block copolymers can direct the room-temperature crystal growth of $BaSO_4$ into novel morphologies. These $BaSO_4$ particles are promising candidates for materials science due to the importance of shape and texture in determining properties of materials.[16] Functionalized polymers extend the possibilities of inorganic morphogenesis,[17] since polyanionic block copolymers are similar to the proteins that organisms use to exert control over biomineral growth[18, 19] and synthetical protein mimics.[20] By varying the binding and solvating blocks in double-hydrophilic block copolymers, more specific templates become available for the formation of complex architectures.

Received: April 27, 1999
Revised: September 13, 1999 [Z13321]

[1] S. Mann, J. Webb, R. J. P. Williams, *Biomineralization, Chemical and Biochemical Perspectives*, VCH, Weinheim, **1989**.
[2] E. Matijevic, *Chem. Mater.* **1993**, *5*, 412 – 426.
[3] S. Weiner, L. Addadi, *J. Mater. Chem.* **1997**, *7*, 689 – 702.
[4] a) M. Sedlak, M. Antonietti, H. Cölfen, *Macromol. Chem. Phys.* **1998**, *199*, 247 – 254; b) M. Sedlak, unpublished results.
[5] H. Cölfen, M. Antonietti, *Langmuir* **1998**, *14*, 582 – 589.
[6] M. Antonietti, M. Breulmann, C. Göltner, H. Cölfen, K. K. W. Wong, D. Walsh, S. Mann, *Chem. Eur. J.* **1998**, *4*, 2493 – 2500.
[7] C. M. Pina, U. Becker, P. Risthaus, D. Bosbach, A. Putnis, *Nature* **1998**, *395*, 483 – 486.
[8] B. R. Heywood, S. Mann, *J. Am. Chem. Soc.* **1992**, *114*, 4681 – 4686.
[9] T. Sugimoto, M. M. Khan, A. Muramatsu, H. Itoh, *Colloids Surf. A* **1993**, *79*, 233 – 247.
[10] D. Shindo, G.-S. Park, Y. Waseda, T. Sugimoto, *J. Colloid Interface Sci.* **1994**, *168*, 478 – 484.
[11] R. Kniep, S. Busch, *Angew. Chem.* **1996**, *108*, 2788 – 2791; *Angew. Chem. Int. Ed. Engl.* **1996**, *35*, 2624 – 2626.
[12] a) S. Busch, Ph.D. thesis, Technische Hochschule Darmstadt, **1998**; S. Busch, H. Dolhaine, A. DuChesne, S. Heinz, O. Hochrein, F. Laen, O. Padebrad, U. Vietze, T. Weiland, R. Kniep, *Eur. J. Inorg. Chem.* **1999**, 1643 – 1653.
[13] R. J. Davey, S. N. Black, L. A. Bromley, D. Cottier, B. Dobbs, J. E. Rout, *Nature* **1991**, *353*, 549 – 550.
[14] M. C. Leeden, G. M. Rosmalen, *J. Colloid Interface Sci.* **1995**, *171*, 142 – 149.
[15] J. D. Hopwood, S. Mann, *Chem. Mater.* **1997**, *9*, 1819 – 1828.
[16] S. Mann, G. A. Ozin, *Nature* **1996**, *382*, 313 – 318.
[17] H. Yang, N. Coombs, G. A. Ozin, *Nature* **1997**, *386*, 692 – 695.
[18] G. Falini, S. Albeck, S. Weiner, L. Addadi, *Science* **1996**, *271*, 67 – 69.
[19] A. M. Belcher, X. H. Wu, R. J. Christensen, P. K. Hansma, G. D. Stucky, D. E. Morse, *Nature* **1996**, *381*, 56 – 58.
[20] J. P. Garris, C. S. Sikes, *Colloids Surf. A* **1993**, *80*, 103 – 112.

  0570-0833/00/3903-0607 $ 17.50+.50/0